This is an *Accepted Manuscript*, which has been through the Royal Society of Chemistry peer review process and has been accepted for publication.

Accepted Manuscripts are published online shortly after acceptance, before technical editing, formatting and proof reading. Using this free service, authors can make their results available to the community, in citable form, before we publish the edited article. We will replace this *Accepted Manuscript* with the edited and formatted *Advance Article* as soon as it is available.

You can find more information about *Accepted Manuscripts* in the **Information for Authors**.

Journal Name

ARTICLE

Unprecedented Transformation of [I⁻·I₃⁻] to [I₄²⁻] Polyiodides in the Solid State: Structure, Phase Transitions and Characterization of Dipyrazolium Iodide Triiodide

M. Węcławik,[a] P. Szklarz,[a] W. Medycki,[b] R. Janicki,[a] A. Piecha-Bisiorek,*[a] P. Zieliński,[c,d] and R. Jakubas[a]

Dipyrazolium iodide triiodide, $[C_3N_2H_5^+]_2[I^-·I_3^-]$, has been synthesized and studied by means of the X-ray diffraction, differential scanning calorimetry, dielectric, and UV-Vis spectroscopy. Two reversible, solid-solid phase transitions (*Imma* (I) ↔ (II) ↔ *Pbam* (III)) at 254 K and 182/188 K respectively, have been revealed. The anionic network experiences spectacular changes associated with a huge rebuilding of the inorganic network from $[I^-·I_3^-]$ to $[I_4^{2-}]$. The low frequency dielectric relaxation process occurrs in phase II with the activation energy of *ca.* 34 kJ/mol. The molecular motions of the pyrazolium cations in $[C_3N_2H_5^+]_2[I^-·I_3^-]$ have been studied by means of proton magnetic resonance (^{1}H NMR). The ferroelastic properties of all phases have been confirmed by polarizing microscopy observations. The molecular mechanism of the phase transitions in the compound is proposed.

Introduction

Molecular ferroics attract increasing attention as potential functional materials. Their possible technological applications in data communication, signal processing, optoelectronics and nonlinear systems.[1-5] are related to reversible phase transitions (PTs) and a characteristic response to external magnetic (ferromagnets), electric (ferroelectrics) or mechanical (ferroelastics) fields. Numerous devices based on phenomena occurring in organic molecules: field transistors (FET), ferroelectric nexus, and parts of data accumulating and storage systems, have been designed in recent years. In comparison with the traditional inorganic oxide materials of the perovskite-type architecture, the materials based on organic molecules and/or ions show relatively low cost of synthesis and of exploitation.

Technologically advanced devices involve very often simple (1:1) two-component molecular-ionic compounds. The best-known systems of this kind are based on protonated aromatic (imidazolium and pyridinium) cations and discrete tetrahedral

anions, such as $[ClO_4^-]$, $[BF_4^-]$, $[IO_4^-]$, $[ReO_4^-]$, $[FSO_3^-]$, or halogen ions ($[Cl^-]$ and $[Br^-]$), which have ferroelectric properties (*e.g.* $[C_3N_2H_5^+][ClO_4^-]$,[11] $[C_3N_2H_5^+][BF_4^-]$,[12] $[C_5N_2H_5^+][IO_4^-]$,[13] $[C_5NH_6^+][ClO_4^-]$,[14] $[C_5NH_6^+][IO_4^-]$,[15] $[C_5NH_6^+][BF_4^-]$,[16] $[C_5NH_6^+][ReO_4^-]$,[17] $[C_5NH_6^+][FSO_3^-]$,[18] and $[C_5NH_6^+][FCrO_3^-]$[19]). In most of these complexes, ferroelectricity appears at low temperatures. However, three imidazolium analogs with $[ClO_4^-]$,[12] $[BF_4^-]$[12] and $[IO_4^-]$[13] counteranions have ferroelectric-type dipolar arrangements at room temperature. The proposed molecular mechanism of the paraelectric-ferroelectric PT seems to be similar in all the solids consisting of the above-mentioned heteroaromatic cations. The onset of ferroelectricity is, namely, governed by the dynamics (ordering) of the organic molecules.

Unique dielectric properties are exhibited by the closely related family of *dabco* monosalts (1,3-diazabicyclo[2.2.2]octane) with tetrahedral anions such as $[ClO_4^-]$, $[BF_4^-]$ and $[ReO_4^-]$, which are room-temperature ferroelectrics.[20,21] Since the $NH^+\cdots N$ hydrogen bonds play a key role in the induction of the ferroelectric properties, these materials are regarded as close analogs of the $OH\cdots O$-bonded KH_2PO_4-type ferroelectrics. In turn, simpler halogen salts based on *dabco* (*e.g. dabco*HCl,[22] *dabco*HBr,[23] *dabco*HI[24], and *dabco*HCl·3H₂O[22]), which are characterized by an analogous topology of hydrogen bonds, are nonpolar, but they were found to show ferroelectric relaxor properties.

These unusual polar properties of simple (1:1) molecular-ionic salts based on aromatic amines motivated the search for ferroelectric properties in different alkylammonium halogen derivatives. Very recently, diisopropylammonium chloride[25] and bromide[26,27] have been found to undergo paraelectric-

a. *Faculty of Chemistry, University of Wrocław, F. Joliot-Curie 14, 50-383 Wrocław, Poland. E-mail: anna.piecha@chem.uni.wroc.pl.*
b. *Institute of Molecular Physics, Polish Academy of Science, Smoluchowskiego 17, 60-179 Poznań, Poland.*
c. *Cracow University of Technology, Institute of Physics, Podchorążych 1, 30-084 Kraków, Poland.*
d. *The H. Niewodniczański Institute of Nuclear Physics, PAS, Radzikowskiego 152, 31-342 Kraków, Poland.*
† Footnotes relating to the title and/or authors should appear here.
Electronic Supplementary Information (ESI) available: [details of: crystal structure, thermal, optical and dielectric properties as well as proton magnetic resonance studies (^{1}H NMR)]. See DOI: 10.1039/x0xx00000x

ferroelectric PT at relatively high temperatures (at 440 and 425 K, respectively). The property that is the most important for technological applications is the value of the spontaneous polarization. The latter, being a result of the ordering of dipolar organic cations,[26,27] amounts to 8.9 μC/cm^2 for the chloride and to 23 μC/cm^2 for the bromide.

The simple ionic molecular iodide analogs have been much less studied due to their weak thermal and chemical stability, as well as to the complex diversity of their polyiodide anions. A large variety of possible anionic networks obtained from simple discrete units through one-, two-, or even three-dimensional sublayers results from both the donor-acceptor interactions and from the influence of counterions.[28]

Many experimental studies have shown that the size, shape, and charge of the associated organic cation have a significant impact on the geometrical features of the polyiodides.[28-31] However, it is still not easy to predict how the ions will modify the physicochemical properties of a compound. For example, we have recently succeeded in obtaining novel imidazolium iodides ([$C_3N_2H_5^+$][I^-] and [$C_3N_2H_5^+$]$_2$[I_4^{2-}]), which, depending on the synthesis conditions, lead to a variety of anionic forms: [I^-] and [I_4^{2-}].[32] At room temperature, [$C_3N_2H_5^+$][I^-] adopts the centrosymmetric, trigonal space group (R-3m). The crystal structure consists of disordered imidazolium cations and discrete [I^-] ions. The compound [$C_3N_2H_5^+$][I^-] undergoes two discontinuous PTs at 180/185 K and 113/123 K (cooling/heating) governed by the imidazolium cation dynamics. The other analog, [$C_3N_2H_5^+$]$_2$[I_4^{2-}], consists of disordered imidazolium cations and of an extremely rare [I_4^{2-}] tetraiodide counterion. It undergoes a continuous PT of the ferroelastic type at 204 K, with symmetry changing from orthorhombic *Fddd* to monoclinic *C*2/c. The mechanism of the PT is complex, with an "order-disorder" contribution assigned to the dynamics of the cations and with a "displacive" contribution causing the distortion of the [I_4^{2-}] rods.

During the reaction of pyrazole ($C_3N_2H_4$, 1,2-diazole) with hydroiodic acid, we succeeded in obtaining compounds characterized by chemical stoichiometry analogous to the imidazole (R) derivative ([R^+]$_2$[I_4^{2-}]), but with a different type of anionic network [$I^-·I_3^-$]. This compound resembles the pyridine analog ([$C_5NH_6^+$]$_2$[$I^-·I_3^-$]) reported by Szafrański *et al.*[33], which shows a similar anionic network and the positional disorder of the pyridinium cations.

The aim of the present paper is to give an account on the physicochemical properties of a novel pyrazolium derivative, [$C_3N_2H_5^+$]$_2$[$I^-·I_3^-$] (abbreviated as PI). We describe its synthesis, single-crystal X-ray diffraction at several temperatures, thermal and dielectric properties. The molecular motions in PI have been studied by means of the proton magnetic resonance measurements (^{1}H NMR). The structure of the ferroelastic domains was determined by optical observations, while UV-Vis spectroscopy has been used to distinguish polyiodide ions with different chain lengths and structures. Finally, the molecular mechanism of the ferroelastic PTs in the compound under investigation is discussed.

Results and Discussion

Thermal properties

Figure 1 shows the DSC traces for PI on cooling and heating at the rate 5 K/min. The calorimetric measurements clearly reveal the existence of two solid-solid reversible PTs. The first heat anomaly, at about 254 K, is characterized by a relatively small temperature hysteresis, (ΔT<1 K), and the lack of the front phase (optical observations). Thus, it may be suggested that this transformation is close to the second-order phase transition. Moreover, the transition entropy (ΔS$_{tr}$), estimated very roughly as being about 2.6 J/mol K, indicates a weak "order–disorder" mechanism of this transition. The strong, first-order PT at low temperatures (182/188 K) is accompanied by an entropy jump of ΔS$_{tr}$=6.5 J/mol K, which is characteristic of an "order–disorder" mechanism. The thermal hysteresis is indicative of the first-order transition. The ΔS$_{tr}$ value was estimated as an average value for the cooling and heating scans for several samples. The error in the estimation of the ΔH and ΔS values is usually as large as 15%–20%. Moreover, the temperature dependence of the linear thermal expansion (see Figure S1– Supplementary Materials) confirms the phase situation detected by the calorimetric measurements. The TGA and DTA analysis show that PI is stable up to about 375 K, and a continuous decomposition of the sample takes place above this temperature (see Figure S2).
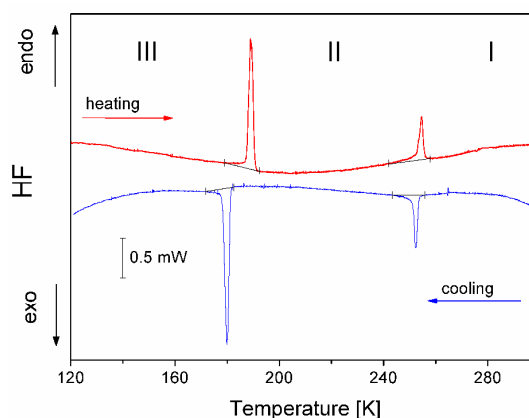
Figure 1 DSC traces for the PI crystal upon cooling and heating runs (5 K/min, m = 12.82 mg).

X-ray Crystal –Structure Analysis

The X-ray diffraction studies of phase I revealed that the room temperature form of PI crystallizes in the orthorhombic space group *Imma* (no. 76). The asymmetric part of the unit cell at 295 K, together with the atom numbering scheme, is represented in Figure 2(a). It consists of one pyrazolium cation characterized by a reorientational disorder (each atom site is occupied by both nitrogen and carbon atoms), one [I^-] anion and half of the [I_3^-] anion. The crystal structure is composed of

Journal Name
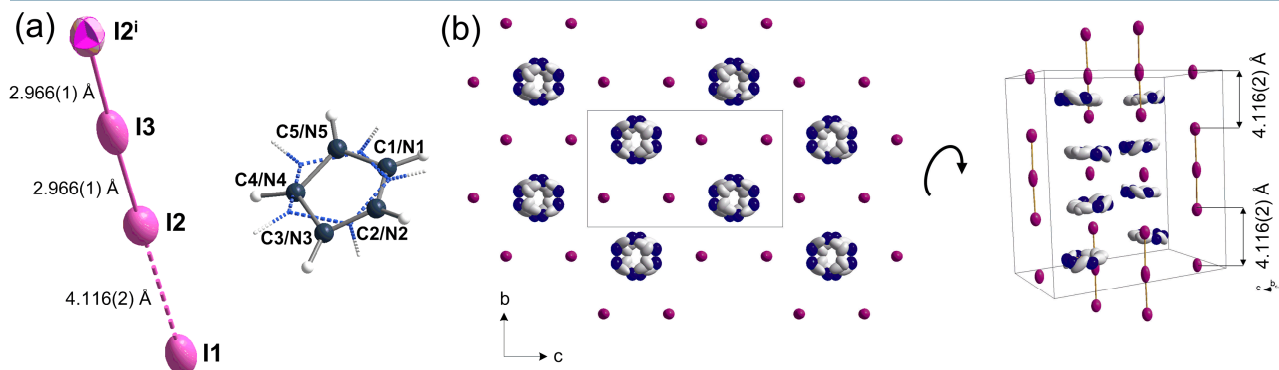
Figure 2 (a) The asymmetric part and atom numbering scheme of PI at 295 K including model of disorder of the pyrazolium counterion together with the structure of [I⁻·I₃⁻] anion (' –x; -y+1/2; z); (b) The crystal packing of PI in the high temperature phase at 295 K (hydrogen atoms are omitted for clarity).

almost linear $[I_3^-]$ and discrete $[I^-]$ anions and, on the other hand, of stacks of pyrazolium cations. The I–I bond lengths of $[I_3^-]$ anions are equal and amount to 2.966 Å, while the I–I–I angle is 178.28° (see Table 1). The discrete $[I^-]$ anions are arranged along the I–I–I axis of the $[I_3^-]$ anions in a similar fashion as in $[I_4^{2-}]$ dianion,[32] but without bonds between them. The distance between the terminal iodide atom of the $[I_3^-]$ anion and the isolated $[I^-]$ is 4.116 Å, which is too long to be regarded as a chemical bond. Nevertheless, the interactions between them should be taken into consideration.

The crystal packing of PI is presented in Figure 2(b). The $[I_3^-]$ and $[I^-]$ anions and the pyrazolium cations stack along the a-axis, that gives rise to a pseudo-hexagonal crystal packing. Such an arrangement of anionic units results in the formation of channels, which are occupied by cationic stacks. The distances between the $[I^-]$ anion and two $[I_3^-]$ anions in the stack are equal.

As a result of the PT at 254 K, the monodomain sample of PI evidently experiences twinning. Such a behavior is in agreement with the optical observations under a polarizing microscope. The presence of an exceptionally fine domain structure in the ab plane suggests a breaking of the crystal symmetry. At this stage of our studies, we were not able to separate two twinned components in the diffraction pattern in the intermediate phase II. Moreover, in phase II we deal with pseudo-merohedral twinning with more than 50% of reflections overlapped. Consequently, our attempt at describing/splitting these two twins has failed. It should be emphasized that the twinning of the sample disappears below the II→III PT temperature (182 K).

In the low-temperature phase III at 100 K, the crystal structure of PI was solved and refined in the orthorhombic space group *Pbam* (No. 55). In this phase, all molecules are ordered. In comparison with the high-temperature phase I, the

unit cell becomes primitive, with doubled volume (doubling of the c cell parameter; see also Table 3 in the Experimental Section). The independent part of the unit cell at 100 K, together with the atom numbering scheme, is presented in Figure 3.

The crucial change in the low-temperature phase involves the anionic unit, $[I^-·I_3^-]$. The distance between the terminal iodide atom of the $[I_3^-]$ anion and the isolated anion $[I^-]$ (I(13)–I(14)) decreases from 4.116(2) Å at 295 K to 3.507(1) Å and 3.481(1) Å at 100 K. This distance is small enough to be considered as a chemical bond. We can firmly state that there is a chemical change/reaction ($[I^-·I_3^-] \rightarrow [I_4^{2-}]$) when approaching the 182 K PT. The product of this reaction is the asymmetric $[I_4^{2-}]$ dianion. The bond lengths (I-I_terminal) are equal to 3.506 Å and 3.280 Å, while the internal I-I bond length is equal to 2.803 Å. The crystal packing of PI at 100 K is presented in Figure 4.
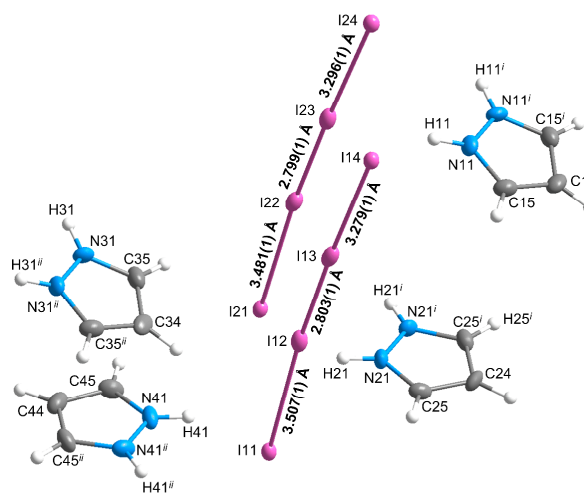

Figure 3 The atom numbering scheme of PI at 100 K. i) x, y, -z; ii) x, y, 1-z.

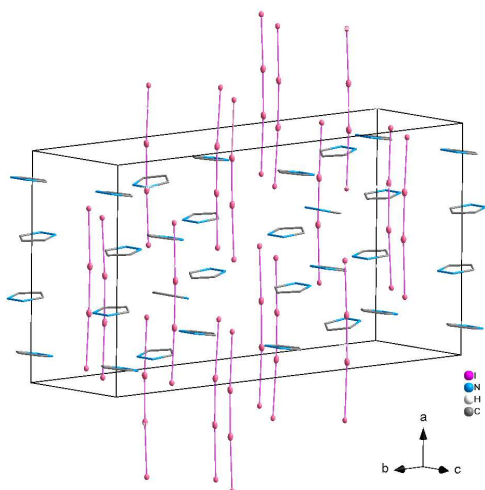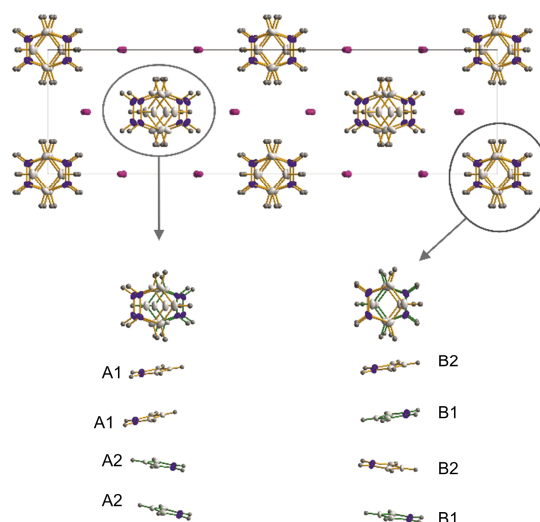**Table 1** Geometry of the anionic structure in phases: I (295 K) and III (100 K).

Phase I [I⁻·I₃⁻]		Phase III [I₄²⁻]	
I(2)-I(3)	2.966(1)	I(11)-I(12)	3.507(1)
I(3)-I(2)ⁱ	2.966(1)	I(12)-I(13)	2.803(1)
I(2)···I(1)	4.116(2)	I(13)-I(14)	3.279(1)
		I(21)-I(22)	3.481(1)
		I(22)-I(23)	2.799(1)
		I(23)-I(24)	3.296(1)
I(2)-I(3)-I(2)ⁱ	178.22(1)	I(11)-I(12)-I(13)	177.70(1)
I(3)-I(2)···I(1)	179.68(1)	I(12)-I(13)-I(14)	176.40(1)
		I(21)-I(22)-I(23)	178.05(1)
		I(22)-I(23)-I(24)	176.66(1)

ⁱ -x, 0.5-y, z

The general crystal structure pattern is the same as in phase I. The $[I_4^{2-}]$ form pseudo-hexagonal channels that are occupied by cationic stacks. Since pyrazolium cations become fully ordered, two different types of stacks can be distinguished (see Figure 5).

In one type of stack (A), two consecutive pyrazolium cations are oriented in the same direction and the next pair of cations are oriented in the opposite direction (···, A1, A1, A2, A2, ···). For the other type of stack (B), the consecutive pyrazolium cations are oriented in the opposite direction (*b* axis) in a "head to tail" arrangement (···B1, B2, B1, B2,···).

The pyrazolium cations are arranged in pseudo-hexagonal channels formed by the $[I_4^{2-}]$ rods. Each cation forms two bifurcated hydrogen bonds with the nearest iodine atom (see Figure 6). The geometric parameters of the hydrogen bonds observed in phase III are presented in Table 2. Pyrazolium carbon atoms do not interact through hydrogen bonds with the $[I_4^{2-}]$ rods.

Figure 5 Two different types of cationic stacks in the low temperature phase of PI at 100 K.

Figure 4 The crystal packing of PI at 100 K (hydrogen atoms are omitted for clarity).

Table 2 Hydrogen bonds PI (Å) and angles (deg) at 100 K

D-H...A	d(D-H)	d(H···A)	d(D···A)	<(DHA)>
N11-H11···I14	0.88	2.85	3.544(3)	136.8
N11-H11···I24	0.88	3.07	3.593(3)	120.4
N21-H21···I11	0.88	2.92	3.531(3)	128.4
N21-H21···I21	0.88	3.01	3.525(3)	119.6
N31-H31···I14ⁱⁱⁱ	0.88	3.02	3.555(3)	121.4
N31-H31···I24ⁱᵛ	0.88	2.84	3.539(3)	137.7
N41-H41···I21	0.88	3.08	3.672(3)	126.1
N41-H41···I11	0.88	3.01	3.528(3)	119.5

ⁱⁱⁱ x-1/2, -y+1/2, -z+1; ⁱᵛ x-1/2, -y-1/2, -z

Figure 6 Hydrogen bonds scheme for two types of channel in PI (phase III). i: x, y, 1+z; ii 0.5+x, 0.5-y, 1-z; iii 0.5+x, 0.5-y, z; iv -0.5+x, 0.5-y, 1-z; v 0.5-x, 0.5+y, -z; vi 0.5-x, 0.5+y, z; vii 0.5-x, 0.5+y, 1-z; viii -0.5+x, 0.5-y, z ix -0.5+x, 0.5-y, -z; x -0.5+x, 0.5-y, 1-z

Figure 7 Absorption spectra of polycrystalline PI compound in polyethylene pellets.

UV-Vis Measurements

Polyiodide anions exhibit a broad spectrum of colors; therefore, UV-Vis spectroscopy seems to be a useful method of characterizing these compounds, in particular to distinguish polyiodide ions of different chain lengths and structures. To confirm the observed PTs, the corresponding structural changes of the absorption spectra at different temperatures have been recorded and presented in Figure 7.

The spectrum of phase I reveals three separate bands centered at 214.8 nm, 289.4 nm, 368.6 nm, and a shoulder at ~468 nm. This spectral pattern is typical of centrosymmetric $[I_3^-]$ anions.[34] The maxima are batochromically shifted as compared to those observed in the spectrum of non-centrosymmetric CsI_3.[36] According to theoretical studies of $[I_3^-]$ anions (symmetry $D_{\infty h}$),[35,36] the ground state configuration is σ^2_u, π^4_u, π^4_g, π^{*4}_u and the LUMO is an antibonding σ^*_u orbital. Two excited configurations belong to the states $^{1,3}\Pi_u(\sigma^2_u, \pi^4_u, \pi^3_g, \pi^{*4}_u, \sigma^2_g, \sigma^{*1}_u)$ and $^{1,3}\Sigma_u(\sigma^2_u, \pi^4_u, \pi^4_g, \pi^{*4}_u, \sigma^1_g, \sigma^{*1}_u)$. The bands at 289.4 nm and 368.6 nm are assigned to the transitions allowed by the symmetry $\pi_g \rightarrow \sigma^*_u$ and $\sigma_g \rightarrow \sigma^*_u$, respectively, while the band at 214.8 nm is attributed to the $\pi \rightarrow \pi^*$ transition of pyrazole. Upon lowering of the temperature, the $[I_3^-]$ anion loses the center of symmetry, and a new band at 467.8 nm appears in the spectrum. Due to the deformation of the $[I_3^-]$ anions, the symmetry-forbidden $\pi_u \rightarrow \sigma^*_u$ transition becomes slightly allowed and appears as a shoulder in the spectra at 263 K and 220 K. The main PT,

observed at 188 K, is associated with the formation of a $[I_4^{2-}]$ anion. However the $[I^- \cdots I_3^-]$ interaction seems to be rather week (I-I bond is equal to 3.506 Å), hence in principle the overall picture of the spectrum do not change significantly. In general an increase of the number of bonded $[I^-]$ brings about an increase of the number of Σ and Π states what gives rise to broadening of the absorption bands due to additional $\sigma \rightarrow \sigma$ and $\pi \rightarrow \sigma$ transitions.[37] The observed extension of the tail of the absorption band reflects the formation of higher polyiodide anions compared to phase I. It is noteworthy that the studied compound displays thermochromism (brown to intense red color) related to the "chemical reaction" $[I_3^-] + [I^-]$ $\leftrightarrow [I_4^{2-}]$ in the solid state.

Optical properties

Figure 8 shows the domain pattern of the PI as seen under polarizing microscopy in the direction perpendicular to the largest face of the relatively thin as grown platelet. The direction perpendicular to the plate is the crystallographic direction [100] in the orthorhombic phases I and III.

The morphology of the plates involves angles close to 60° or 120° that reflect the molecular architecture in which the iodide chains as well as the pyrazolium rings form distorted hexagons. Figures 8(a) and 8(b) show a number of readily flat domain walls. The angle between these domain walls (60°), bisected by the crystallographic direction [001], is very close to the angle formed by the diagonals of the base rectangle (b,c) in phase I. This suggests that the domains in phase I are separated by stress-free twin domain walls of this orthorhombic phase. The difference between the domains would disappear if the structure became strictly hexagonal. Therefore, we can state that this domain pattern is a trace of a hexagonal prototype phase, not observed at least at ambient pressure.
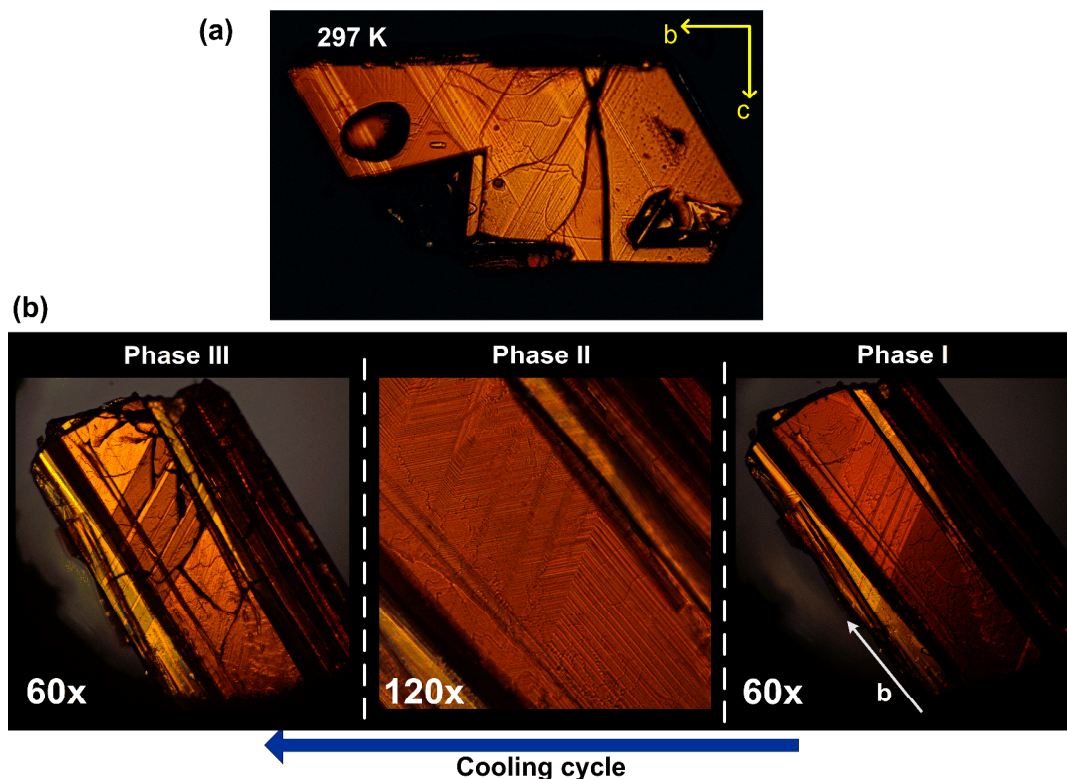
Figure 8 (a) Domain pattern of PI in phase I; (b) evolution of the domain pattern during cooling of the sample ((a) and (b) photos were taken on different samples).

A new, even finer, domain structure arises in phase II (see Figure 8(b)). The domain walls are practically parallel to the crystallographic direction [010] as counted in phase I. This indicates that the mirror plane (001) and the two-fold axis [001] (still referred to the orthorhombic system) are lost as symmetry elements in this phase transition. We can interpret this symmetry reduction as a change of the crystallographic system.

Observations of domain walls in phase III show the disappearance of the above domains. Another, strongly pronounced domain structure surviving in all phases is observed in the material under a shear stress applied to the edges of the plates. An example (Figure S3) is given in the Supplementary Material.

Dielectric properties

The measurements of the complex dielectric permittivity, ε^*, of PI as a function of temperature (100–300 K) and frequency (135 Hz–2 MHz) were carried out along the a-axis. Figure 9 shows the temperature dependence of the real part of the complex electric permittivity, ε_a', below room temperature upon first cooling. At the PTs temperatures (254 and 182 K) discontinuous changes in the dielectric permittivity value are observed, which are perfectly reversible on heating. The observed dielectric increments ($\Delta\varepsilon_a$) for the transitions: I → II (Figure 9(a)) and II → III (Figure 9(c)) amount to 1.5 and 0.75, respectively.

It should be emphasized that the dielectric response in PI is quite complicated. Dielectric measurements carried out for numerous single-crystal and pellet samples (see Figure S4) showed that, between 300 and 100 K, four relaxation processes (relaxators) appear in the following phases. The dielectric increment of these relaxators significantly depends on the quality and distortion of the sample, which are connected with the domain wall state. It should be noted that for some samples four or three relaxators are visible. The relaxator in phase II is usually well shaped and characterized by the highest increment in comparison to the others. The properties of this relaxator are analyzed in detail below.

Figure 9(b) shows the temperature dependence of the imaginary part of the complex electric permittivity (ε_a''). Over the low-temperature phase II, a relaxation process in the radio-frequency region (8.9 kHz– 2 MHz) is observed which is well described by the Cole–Cole relation (Eq. 1)

$$\varepsilon^*(\omega) = \varepsilon_\infty + \frac{\varepsilon_o - \varepsilon_\infty}{1 + (i\omega\tau)^{1-\alpha}} \quad (Eq.\,1)$$

where: ε_0 and ε_∞ are the low- and high-frequency limits of dielectric permittivity, respectively; ω is angular frequency; and τ is the macroscopic relaxation time.

We fitted the experimental Cole-Cole plots at several temperatures with Eq. (1) and determined the fitting parameters ε_0, ε_∞ and τ (see Figure S5). In the crystals characterized by weak dipole-dipole interactions, one can assume that the macroscopic relaxation time (τ) may be identified with the microscopic (τ_0) one.
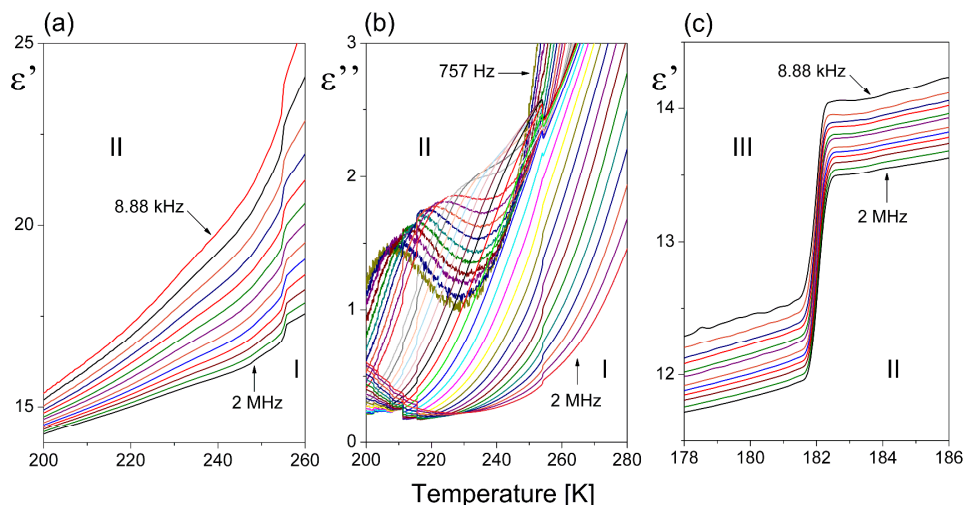
Figure 9 The temperature dependence of the (a) real (ε') and (b) imaginary, (ε'') parts of the complex dielectric permittivity, at selected frequencies along the *a*-axis for PI upon cooling in the vicinity of I $\rightarrow$ II PT. (c) Response of the dielectric permittivity (ε' (T, ω)) in the vicinity of II$\rightarrow$III PT.

Thus, the energy barrier E_a can be estimated from the Arrhenius relation:

$$\tau = C \exp\left(\frac{E_a}{kT}\right) \qquad (Eq.\,2).$$

The magnitude of E_a (being 34 kJ/mol) is found to be large (see Figure S6) as for the rather small size of the pyrazolium cation. This result may be explained by the fact that the organic dipole, $[C_3N_2H_5^+]$, contributing to the electric polarization of the title crystal is strongly stiffened in the crystal lattice.

Proton Magnetic Resonance studies (^{1}H NMR)

The measurements of the temperature dependence of the spin–lattice relaxation time (T_1) of PI are presented in Figure 10(a). In the studied temperature range, the only one-exponential recovery of magnetization was found. On heating (from 90 K), one can observe a slight decrease in the T_1 relaxation time and above 145 K the experimental points start to form the right-hand side of a relaxation time minimum, not fully shaped due to the PT at 188 K. From this temperature, the relaxation time continuously increases with small activation energy of the order of 2.8 kJ/mol. Above 246 K, the steep slope of the left-hand side of the relaxation time minimum is found with a rather high value of activation energy (29.3 kJ/mol).

The detailed analysis of the T_1 relaxation time behavior, in the temperature range between 90 and 300 K, was carried out analogously to the corresponding ionic crystals based on the 1-aminopyridinium cation[38] or imidazolium[39] one. As described in references,[38,39] the relaxation process over a broad temperature range consists of two distinct types of mechanisms: one is attributed to the classical (^{1}H–^{1}H) dipole–dipole interactions, while the other to an interaction between hydrogen and iodide quadrupole nuclei (^{1}H–^{127}I). The characteristic plateau observed at low temperatures (Figure 10(a)) corresponds to the second relaxation mechanism (^{1}H–

^{127}I interactions), whereas the onset of the appearing of a relaxation minimum before the PT is a result of the domination of the classical relaxation mechanism (dipole-dipole interactions) at higher temperatures. For that reason, the fitting procedure of T_1 includes the sum of both of the considered components,[38-42] (Eq. 3), where ω_I is the Larmor frequency of ^{127}I. The correlation times, $\tau_{c,Q}$, are defined as: $\tau_{c;Q}^{-1} = \tau_c^{-1} + R_Q$, where R_Q represents the quadrupolar spin–lattice rates of ^{127}I.

The parameters of Eq. (3) fitted to the experimental data (red line in Figure 10(a)) are the following: E_a = 11.2 kJ/mol, τ_c = 1.9 10^{-12} s, the C_{HH} = 5.6 10^6 s^{-2}, C_{HI} = 8.6 10^5 s^{-2} and R_Q^{-1}=8.1 10^{-9} s . As expected, the coefficient C_{HI} is significantly smaller than C_{HH} because of the gyromagnetic factor of ^{127}I and of the structure of the compound, while the time scale of the quadrupolar relaxation is plausible because of the very strong quadrupolar coupling of ^{127}I.

The quadrupolar relaxation has been assumed to be temperature independent. The contribution of the effective modulations of the ^{1}H–^{127}I dipole–dipole coupling makes the ^{1}H relaxation time constant (the plateau in Figure 10(a)) although the correlation time τ_c becomes very long at low temperatures. The obtained lower values of activation energy and a longer correlation time than that reported[40,41] may result from the fact that the relaxation time T_1 at low temperatures is five times longer giving a smaller value of the relaxation constants C_{HH} and C_{HI}.

The temperature dependence of the second moment M_2 of the ^{1}H NMR line of PI is presented in Figure 10(b). The dashed vertical lines represent the temperature points of the PTs detected by the thermal methods. Upon heating (from 101 K), the ^{1}H M_2 values decrease gradually from *ca.* 14.6×10^{-8} T^2 to 9.6×10^{-8}T^2 (at about 240 K). It should be emphasized that a step-wise decrease in the M_2 value, down to 2.7×10^{-8} T^2, close to the PT (II $\rightarrow$ I), is observed. On the other hand, no change in M_2 was found at $T_{c(III\rightarrow II)}$=188 K.
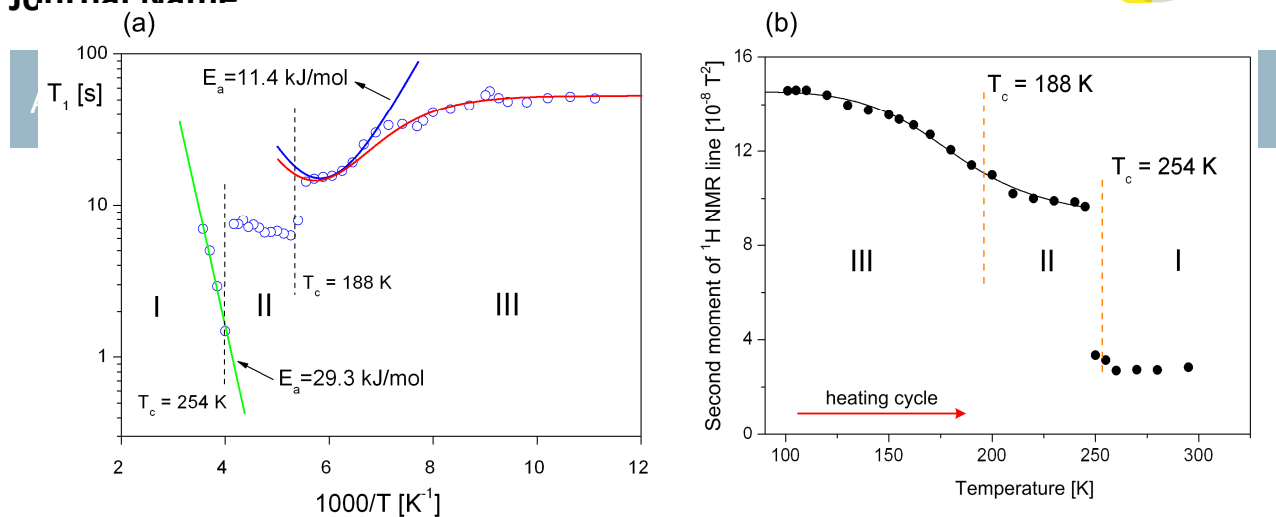
Journal Name

Figure 10 (a) Temperature dependence of the spin-lattice relaxation time (T$_1$) of ^{1}H NMR. The red solid line represents fitting to a minimum with added very strong quadrupolar mechanism; (b) temperature dependence of the line width (M$_2$) of the ^{1}H NMR spectrum.

$$\frac{1}{T_1} = C_{HH}\left[\frac{\tau_c}{1+\omega_H^2\tau_{ci}^2} + \frac{4\tau_c}{1+4\omega_H^2\tau_c^2}\right] + C_{HI}\left[\frac{\tau_{c,Q}}{1+(\omega_H-\omega_I)^2\tau_{c,Q}^2} + \frac{3\tau_{c,Q}}{1+4\omega_H^2\tau_{c,Q}^2} + \frac{6\tau_{c,Q}}{1+(\omega_H+\omega_I)^2\tau_{c,Q}^2}\right] \ (Eq.\,3)$$

The smooth reduction of the second moment found between 101 and 240 K may witness to its temperature dependence as

$$M_2 = M_2 + (M_2 + M_2)\frac{2}{\pi}arctg(\gamma_H\sqrt{M_2}\tau_c) \ (Eq.4)$$

it follows from the BPP formula[43,44] where: the correlation time follows the Arrhenius law, τ_c= $\tau_0$exp(E$_a$/RT); M$_{2rigid}$ and M$_{2motion}$ are the second moment values before (rigid) and after (motion) the onset of a given type of motion, respectively. A numerical fit has provided the following parameters: M$_{2rigid}$ = 14.5 × 10–8 T2, M$_{2motion}$ = 8.7 × 10–8 T2, E$_a$ = 8.3 kJ/mol and τ_{c0} = 4.95·10^{-8} s (see the fitting curve in Figure 10(b)). These parameters correspond to a relatively slow motion with a small activation energy that suggests that the relaxation process originates from a gradual elongation of the lengths of the H–H bonds with respect to the distance usually observed (see the Supplementary Materials for details). This effect may be a result of the weakening of the H-bond, N-H···I. The observed jump at the PT temperature results in the reduction of M$_2$ by a quarter, which excellently confirms the onset of the in-plane reorientation around the pseudo-C$_5$ axis of the pyrazole ring.

Discussion

In general, all of the experimental methods used indicate a complex mechanism of the structural PTs in PI. The mechanism is postulated to involve two different contributions. The calorimetric measurements revealed that the transition entropy (ΔS_{tr}) accompanying both PTs was characteristic of an "order-disorder" mechanism, while the mutual displacement

of the [I$_3$$^-$] and [I$^-$] ions within the anionic chains indicates presence of a "displacive" contribution.

It should be emphasized that PI may be classified as a ferroic crystal. This is implied by the fact that PI exhibits a ferroelastic domain structure for all of the temperatures studied. Additionally, the presence of ferroelastic properties in phase I suggests that, at higher temperatures, we could expect the prototypic (paraelastic) phase, which is not really attained before the decomposition of the sample, which takes place above 375 K. On the other hand, a clear rebuilding of the domain wall configurations below 254 K (on cooling) corroborates the observed symmetry reduction. Both PTs are dielectrically active: at the lower-temperature transition II→III, only a subtle step-wise change in the electric permittivity ($\Delta\varepsilon \approx$ 0.75) was recorded, whereas the dielectric anomaly close to the PT I→II is characterized by a distinctly larger dielectric increment ($\Delta\varepsilon \approx$ 1.5). Within the intermediate phase II, a low-frequency dielectric relaxation process was detected, which confirms the presence of dipolar motions assigned to the dynamics of pyrazolium cations.

It should be emphasized that the dynamic properties of the intermediate phase II are still poorly characterized. Both PTs were clearly visible in the T$_1$ relaxation time measurements because they were accompanied by a significant jump in T$_1$ exactly at the critical points. On the other hand, in the second moment measurements, only the higher-temperature PT was active (a drastic reduction of M$_2$), while the PT at 188 K was not visible. Nevertheless, one can conclude that the PT II→I was accompanied by a rapid release of the pseudo-C$_5$-type motion of the pyrazolium cations. This is consistent with a
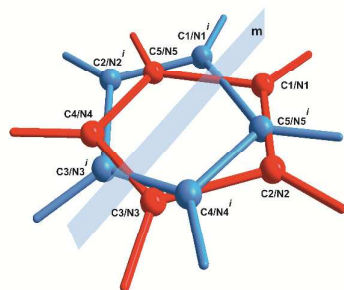
Figure 11 Model of disorder of the pyrazolium cation in the phase (I).

large activation energy value above 254 K (*ca.* 29 kJ/mol), which is a characteristic value for the overall reorientation of pentagonal or hexagonal heteroaromatic rings. The markedly smaller value of E_a for the lowest-temperature phase III in comparison to phase I indicates that there was a drastic change in the motional state of the organic cations. On the other hand, the lack of anomalous changes in M_2 through the PT II→III suggests that the slowing of the motion of pyrazole rings was extended over a wider temperature range. Additionally, the PT II→III was probably governed mainly by the distortions of the anionic network ("displacive" contribution).

Single-crystal X-ray diffraction showed that two PTs taking place in PI were accompanied by significant changes in the crystal structure. To characterize the structural features of the two PTs, it was necessary to consider all the disordered molecules and the symmetry changes between consecutive phases (also see Figure S8). In the high-temperature phase I, pyrazolium cations exhibited a clear reorientational disorder. A detailed analysis of the geometrical distances between the atoms in the pyrazolium ring and the nearest environment (hydrogen bonds to iodide atoms) did not show any preferences that could unequivocally identify the atom type. In this case, we assumed that each pyrazolium ring atom site was occupied by both carbon and nitrogen atoms, in 60%:40% proportion, respectively. Moreover, the *m* mirror symmetry plane crossed perpendicularly to the pyrazolium molecule and generated the two other symmetry equivalent positions set (see Figure 11).

This model of disorder, large temperature displacement coefficients and values of entropy change accompanying the PT unequivocally indicated that pyrazolium cations in phase I perform free in-plane rotations. This supposition was confirmed by the ^{1}H NMR results. All the iodide atoms in phase I are ordered and lie on the mirror symmetry planes. The iodide atoms were arranged in almost linear [I_3^-] anions and free [I^-] ions. The centers of all the iodide atom of [I_3^-] and the free [I^-] atom lie at the intersection of two *m* planes (see Figure 12). In low-temperature phase III, the mirror symmetry planes parallel to pyrazolium stacks disappeares. The free [I^-] ions join the [I_3^-] ions to form [I_4^{2-}] ions. The resulting [I_4^{2-}] ionic rods lay on the *m* mirror planes and, in comparison to the [I_3^-] ions, were considerably bent (Figure 12). Such a deformation results
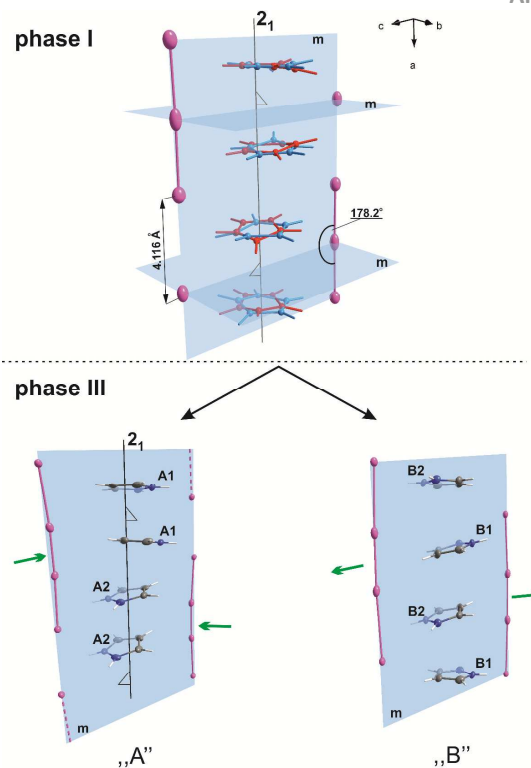

Figure 12 Symmetry changes between phases I and III in PI.

in the appearance of two types of pseudohexagonal channels. In the first type, the [I_4^{2-}] rods are bent inside the channel. In the second type, the [I_4^{2-}] rods are bent outside the channel (see Figure 13). This distortion explains the two types of cationic stacks with different sequences of pyrazolium cations.

It will be interesting to compare the structural and dynamic properties of three closely related compounds having an identical amine-to-iodide ratio (R:I = 2:4 (R- amine)) and comparable organic cation size and symmetries: ([$C_5NH_6^+$]$_2$[$I^- \cdot I_3^-$]) (pyridinium), [$C_3N_2H_5^+$]$_2$[I_4^{2-}] (imidazolium), and pyrazolium (PI)). The compound under investigation (PI) exhibited an intermediate structural motif of the anionic network between those of the first and the second analyzed compounds since the anionic network was modified with temperature.

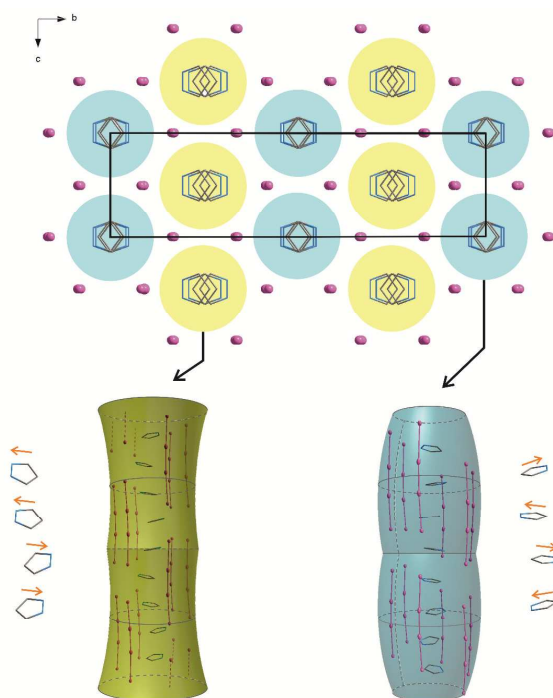The phase situation for these three compounds is illustrated in the following diagram:
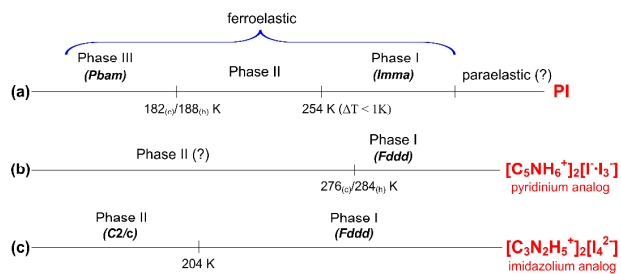
Figure 13 Structure arrangement and two types of channels in phase (III).

It should be emphasized that $[C_3N_2H_5^+]_2[I_4^{2-}]$ (imidazole) and PI (pyrazole) are characteristic examples of an ionic salt among all of the known compounds (14)[39] containing polyiodide anions ($[I_4^{2-}]$), which undergo structural PTs. In both cases, the proton spin-lattice relaxation time (T_1) measurements confirmed, that a free in-plane reorientation of the imidazolium ring took place in phase I, whereas large-amplitude librations or small-angle reorientations of cations (in PI) occurred at low temperatures. Similarly, in the $[C_5NH_6^+]_2[I^-\cdot I_3^-]$ (pyridinium) analog, the room-temperature phase was characterized by a free C_6'-type reorientation of the hexagonal ring. The I→II PT at 276 K (on cooling) was accompanied by a rapid freezing-out of dipolar cations. All compounds from this group exhibited a low frequency dielectric relaxation process, which confirms the dynamics of the dipolar cations.

The common feature of the analyzed compounds was the fact that, apart from an "order-disorder" contribution (cationic moieties), the low temperature PT mechanism involved an essential "displacive" factor (distortion of $[I_4^{2-}]$ or $[I^-\cdot I_3^-]$ anions).

The presented spectroscopic results seem to be in agreement with the single-crystal X-ray diffraction data, thus allowing us to propose the molecular mechanism of PTs in the PI analog.

Conclusions

In summary, we have reported a novel molecular-ionic compound (dipyrazolium iodide triiodide $[C_3N_2H_5^+]_2[I^-\cdot I_3^-]$) built of pyrazolium cations and polyiodides counterions, and characterized by an atypical sequence of structural PTs: orthorhombic (*Imma*: (I)) ⇔ (II) ⇔ orthorhombic (*Pbam*: (III)). The title crystal was classified as a ferroic material that shows ferroelastic properties over all phases.

An extraordinary result from the perspective of the structural properties was the fact that the anionic network experienced a huge rebuilding between phases I and III, since it changes from $[I^-\cdot I_3^-]$ to $[I_4^{2-}]$. Such an effect, which was confirmed by the UV-Vis measurements, was observed for the first time in polyiodide analogs and refers to a chemical reaction in the solid state.

The mechanism of PTs is complex because it involves at the same time an ordering of a reorientational motion of pyrazolium cations (an "order-disorder" contribution) and a reorganization of the iodide atoms in the anionic moieties (a "displacive" contribution). The "order-disorder" contribution to the mechanism of PT at 254 K was confirmed by the thermal (DSC) and ^{1}H NMR spectroscopy. However, the value of ΔS from calorimetric studies suggests a "mixed" mechanism of this transition because it is distinctly larger than that usually encountered in crystals with a "pure" displacive mechanism (usually $\Delta S \langle$ 0.5 J/mol K). The dielectric relaxation and ^{1}H NMR suggest that changes in the dynamics of dipolar organic cations take place over the wide temperature region.

Our experimental results show that even the simplest molecular-ionic salts should be taken into consideredation in the strategy of searching for promising, smart and functional materials.

Acknowledgements

Experimental

Synthesis of the complex

All materials used in this work were of reagent grade purity and were used as commercially obtained: pyrazole (Acros Organics, 98%) and HI (Merck, 57%).

The crystalline $[C_3N_2H_5^+]_2[I^-\cdot I_3^-]$ compound were prepared with the access to air.

The concentrated HI (3.9 ml, 0.02955 mol) was added dropwise to a stirred solution containing pyrazole (1 g, 0.0147 mol) in H_2O (5 ml) at 25°C. After a few days single crystals of $[C_3N_2H_5^+]_2[I^-\cdot I_3^-]$ (PI) were grown by slow evaporation from the red solution. The crystalline product was twice recrystallized from water. Single red, platelet like, crystals were

characterized by an elemental analysis: C: 11.17% (theor. 11.16%), N: 8.61% (theor. 8.68%), H 1.23% (theor. 1.56%).

General

DSC (Differential Scanning Calorimetry) heating traces were obtained using a Perkin Elmer model 8500 differential scanning calorimeter calibrated using n-heptane and indium. Hermetically sealed Al pans with the polycrystalline material were prepared in a controlled-atmosphere N_2 glovebox. The measurements were performed between 100 and 300 K The thermal hysteresis was estimated from the scans performed at various rates (20, 10 and 5 K/min) extrapolated to a scanning rate of 0 K/min.

The dilatometric measurements were carried out a thermomechanical analyzer Perkin Elmer TMA-7 in the temperature range 100-300 K (more information in Supplementary Materials).

Simultaneous Thermogravimetric Analysis (TGA) and **Differential Thermal Analysis (DTA)** were performed on Setaram SETSYS 16/18 instrument in the temperature range 300-750 K with a ramp rate 2 K/min, the scans were performed in flowing nitrogen (flow rate: 1 dm^3/h).

The complex dielectric permittivity, $\varepsilon^* = \varepsilon' - i\varepsilon''$ was measured between 100 and 290 K by the Agilent 4284A Precision LCR Meter in the frequency range between 135 Hz and 2 MHz. The overall error was less than 5%. The single crystal samples had dimensions *ca*. 5 x 3 x 1 mm^3. Cuprum electrodes were sticked on the opposite faces. The sample before measurements was kept at 310 K and blown dry with dry nitrogen for 2 h. The dielectric measurements were carried in a controlled atmosphere (N_2).

NMR measurements were made using an ELLAB TEL-Atomic CWS 12-50 spectrometer. The second moment of ^{1}H NMR (see Supporting Information) line was measured in temperature range from 101 to 295 K by a continuous wave spectrometer working on protons at the frequency of 28.2 MHz. The second moment values were found by numerical integration of the absorption curve derivatives. T_1 relaxation times (^{1}H NMR) in temperature range from 90 K to 280 K were measured with ELLAB TEL–Atomic PS 15 spectrometer working at the frequency of 15 MHz. The temperature of the sample was controlled by a UNIPAN 660 temperature controller operating on Pt 100 sensor providing long time temperature stability better than 1 K. All measurements were made on heating the sample from liquid nitrogen temperature. The errors in the measurements of T_1 were estimated to be about 5%. The sample were degassed at room temperature and sealed under vacuum in glass ampoule.

The absorption spectra of PI compound were recorded with a Cary 5000 UV/Vis/NIR. The spectra of PI powder in polyethylene pellets were measured at different temperatures (160-293 K) in a continuous flow helium cryostat (Optistat, Oxford). The spectra were corrected by the subtracting the background of polyethylene pellets with the same thickness.

The crystallographic measurements were performed on a Xcalibur, Sapphire2 four-circle diffractometer with the graphite-monochromatized MoKα radiation. The data for the crystal were collected at 100(2) and 295(2) K using the Oxford Cryosystems cooler and were analytically corrected for absorption with the use of CrysAlis RED program of the Xcalibur software, using a multifaceted crystal model based on expressions derived by Clark and Reid[45]. A summary of the conditions for the data collection and the structure refinement parameters are given in Table 3. The structures were solved by the heavy atom method using the SHELXS-2013 program and refined by the full-matrix least-squares technique using SHELXL-2013[46] with anisotropic thermal parameters for non-H atoms. The hydrogen atoms were treated as riding atoms and refined with N–H and C–H distances fixed (at 0.88 and 0:95A°, respectively) and with isotropic temperature factors Uiso assumed as 1.2 times Ueq of their closest heavy atoms. Crystallographic data for the structure reported in this paper have been deposited with the Cambridge Crystallographic Data Centre, CCDC numbers: 1022215 and 1022217. Copies of this information may be obtained free of charge from the Director, CCDC, 12 UNION Road, Cambridge CB2 1EZ. UK (fax: +441223 336033; e-mail: deposit@ccdc.cam.ac.uk or http://www.ccdc.cam.ac.uk).

The optical observations The ferroelastic domain structure of the PI crystal was studied by means of an Olympus BX53 optical polarization microscope. The samples were placed in a LINKAM THM-600 heating/cooling stage, where the temperature was stabilized to within 0.1 K.

Table 3 Experimental data for $[C_3N_2H_5^+]_2[I^-\cdot I_3^-]$

	Phase I	Phase III
Empirical formula		$C_6H_{10}I_4N_4$
M_w		645.78
Crystal system	Orthorombic	Orthorombic
Space group	*Imma*	*Pbam*
a [Å]	14.162(6)	13.884(4)
b [Å]	7.913(3)	27.640(8)
c [Å]	13.627(4)	7.651(3)
V [Å^3]	1527.1(10)	2936.1(17)
Z	4	8
ρ_{calc} [Mg/m^3]	2.809	2.922
Absorption coefficient [mm^{-1}]	8.139	8.467
F(000)	1144	2288
Crystal size [mm]	0.276x 0.172x 0.096	0.234x 0.151x 0.093
Wavelenght [Å]		0.71073
T [K]	295(2)	100(2)
Theta range for data collection	2.877 - 36.760°	2.934 - 28.749°
	-18 ≤ h ≤ 23	-18 ≤ h ≤ 18
	-12 ≤ k ≤ 10	-34 ≤ k ≤ 35
Index ranges	-16 ≤ l ≤ 22	-9 ≤ l ≤ 9
Reflections collected	8764	23766
Independent reflections	1847 [R(int) = 0.0316]	3899 [R(int) = 0.0343]
Completeness to theta = 27.000°	99.8 %	99.7%
Refinement method		Full-matrix least-squares on F^2
Data / restraints / parameters	1847 / 23 / 61	3899 / 0 / 146
Goodness-of-fit on F^2	1.005	1.030
Final R indices [I>2sigma(I)]	R1 = 0.0392, *w*R2 = 0.0950	R1 = 0.0267, *w*R2 = 0.0575
R indices (all data)	R1 = 0.0765, *w*R2 = 0.1143	R1 = 0.0388, *w*R2 = 0.0604
Extinction coefficient	0.0046(3)	0.000252(18)
Largest diff. peak and hole [eÅ^3]	1.032 and -1.030	0.995 and -1.258

References

1 J. F. Scott, C. A. P. Araujo, *Science* 1989, **246**, 1400;
2 J. F. Scott, *Science* 2007, **315**, 954;
3 Z. Wen, C. Li, D. Wu, A. Li, N. Ming, *Nat. Mater.* 2013, **12**, 617;
4 B. Cho, T.-W. Kim, S. Song, Y. Ji, M. Jo, H. Hwang, G.-Y. Jung, T. Lee, *Adv. Mater. 2010*, **22**, 1228;
5 J. C. Scott, L. D. Bozano, *Adv. Mater.* 2007, **19**, 1452;
6 R. Jakubas, A. Piecha, A. Pietraszko, G. Bator, *Phys. Rev. B* 2005, **72**, 104107-1;
7 A. Piecha, A. Białońska, R. Jakubas, *J. Phys. Condens. Matter* 2008, **20**, 1;
8 A. Piecha, A. Pietraszko, G. Bator, R. Jakubas, *J. Solid State Chem*. 2008, **118**, 1155;
9 A. Piecha, A. Białońska, R. Jakubas, *J. Mater. Chem*. 2012, **22**, 333;
10 J. Jóźków, R. Jakubas, G. Bator, A. Pietraszko, *J. Chem. Phys.* 2001, **114**, 7239;
11 Z. Pająk, P. Czarnecki, B. Szafrańska, H. Małuszyńska, Z. Fojud, *J. Chem. Phys.* 2006, **124**, 1;

Dalton Transactions Accepted Manuscript

ARTICLE

12 Z. Pająk, P. Czarnecki, B. Szafrańska, H. Małuszyńska, Z. Fojud, *Phys. Rev*. B 2004, **69**, 1;

13 Y. Zhang, H.-Y. Ye, H.-L. Cai, D.-W. Fu, Q. Ye, W. Zhang, Q. Zhou, J. Wang, G.-L. Yuan, R.-G. Xiong *Adv. Mater.* 2014, **26**, 4515;

14 P. Czarnecki, W. Nawrocik, Z. Pajak, J. Wąsicki, *J. Phys. Condens. Matter*, 1994, **6**, 4955;

15 Z. Pająk, P. Czarnecki, J. Wąsicki, W. Nawrocki *J. Chem. Phys*. 1998, **109**, 6420;

16 P. Czarnecki, W. Nawrocik, Z. Pajak, J. Wąsicki, *J. Phys. Rev. B*, 1994, **49**, 1511;

17 J. Wąsicki, P. Czarnecki, Z. Pająk, W. Nawrocki, W. Szczepański *J. Chem. Phys*. 1997, **107(2)**, 576;

18 Z. Pająk, P. Czarnecki, H. Małuszyńska, B. Szafrańska, M. Szafran, *J. Chem. Phys*. 2000, **113**, 848;

19 Z. Pająk, H. Małuszyńska, B. Szafrańska, P. Czarnecki *J. Chem. Phys*. 2002, **117**, 5303;

20 A. Katrusiak, M. Szafrański, *Phys. Rev. Lett*., 1999, **82**, 576;

21 M. Szafrański, A. Katrusiak, G. J. McIntyre, *Phys. Rev. Lett*., 2002, **89**, 215507-1;

22 M. Szafrański, *J. Mater. Chem. C*, 2013, **1**, 7904;

23 M. Szafrański, *J. Phys. Chem. B*, 2009, **113**, 9479;

24 M. Szafrański and A. Katrusiak, *J. Phys. Chem. B*, 2008, **112**, 6779;

25 D.-W. Fu, W. Zhang, H.-L. Cai, J.-Z. Ge, Y. Zhang, R.-G. Xiong, *Adv.Mater.* 2011, **23**, 5658;

26 A. Piecha, A. Gągor, R. Jakubas, P. Szklarz, *CrystEngComm.* 2013, **15**, 940;

27 D.-W. Fu, H.-L. Cai, Y. Liu, Q. Ye, W. Zhang, Y. Zhang, X.-Y. Chen, G. Giovannetti, M. Capone, J. Li, R-G. Xiong *Science* 2013, **339**, 425;

28 P. H. Svensson, L. Kloo, *Chem Rev*., 2003, **103**, 1649 and references cited therein;

29 A. J. Blake, R. O. Gould, S. Parsons, C. Radek, M. Schröder, *Angew. Chem., Int. Ed. Engl.* 1995, **34**, 237;

30 S. Silvi, M. Venturi, A. Credi, *J. Mater. Chem*. 2009, **19**, 2279;

31 C. He, D. A. Parrish, J. M. Shreeve *Chem. Eur. J.* 2014, **20**, 6699;

32 M. Węcławik, A. Gągor, A. Piecha, R. Jakubas, W. Medycki *CrystEngComm.* 2013, **15**, 5633;

33 M. Szafrański, H. Małuszyńska and I. Szafraniak, *Ferroelectrics*, 2002, **268**, 289;

34 W. Gabes, D. J. Stufkens, *Spectrochimica Acta A*, 1974, **30**, 1835;

35 A. S. Pereira Gomes, L. Visscher, H. Bolvin, T. Saue, S. Knecht, T. Fleig, E. Eliav, *J. Chem. Phys.*, 2010, **133**, 064305;

36 R. Nakanishi, N. Saitou, T. Ohno, S. Kowashi, S. Yabushita, T. Nagata, *J. Chem. Phys.*, 2007, **126**, 204311;

37 P. H. Swensson, L. Kloo, *Chem. Rev.*, 2003, **103**, 1649;

38 M. T. Owczarek, R. Jakubas, V. Kinzhybalo, W. Medycki, D. Kruk, A. Pietraszko, M. Gałązka, P. Zieliński *Chem. Phys. Lett*., 2012, **537**, 38;

39 M. Węcławik, A. Gągor, A. Piecha, R. Jakubas, W. Medycki *CrystEngComm.*, 2013, **15**, 5633;

40 D. Kruk, O. Lips *SSNMR*, 2005, **28**, 180;

41 D. Kruk, W. Medycki, A. Mielczarek, R. Jakubas, C. Uniszkiewicz, *Appl. Magn. Reson*., 2010, **39**, 233;

42 D. Kruk, O. Lips, *J. Magn. Reson.,* 2006, **179**, 250;

43 A. Abragam, *The Principles of Nuclear Magnetism*, Clarendon Press, Oxford, 1961;

44 C. P. Slichter, *Principles of Magnetic Resonance*, Springer-Verlag, Berlin,1990;

45 R. C. Clark and J. S. Reid, *Acta Cryst. A*, 1995, **51**, 887-897;

46 G. M. Sheldrick, *Acta Cryst. A*, 2008, **64**, 112.